Fully coupled thermo-hydro-mechanical model with oversaturation and its validation to experimental data from FEBEX experiment

Zdeněk Michalec, Radim Blaheta, Martin Hasal, Tomáš Ligurský

Fully coupled thermo-hydro-mechanical model with oversaturation and its validation to experimental data from FEBEX experiment

Z. Michalec, R. Blaheta, M. Hasal, T. Ligurský

Affiliation: Institute of Geonics of the Czech Academy of Sciences, Ostrava, Czech Republic

Corresponding author: Radim Blaheta, e-mail: radim.blaheta@ugn.cas.cz, telephone: +420-603450245

Dedication: This paper is dedicated to the memory of Professor Ove Stephansson, an outstanding scientist in the field of rock mechanics and one of the founders of the DECOVALEX research project. We are very thankful to him for inspiration and friendship.

Abstract: The paper is devoted to the formulation of a mathematical model which enables analysis of coupled thermo-hydro-mechanical (THM) processes with a special focus on processes in bentonite and bentonite-based sealing barriers which are component of designs of deep geological repositories for a high-level radioactive waste including the spent nuclear fuel. Such modelling is important as the analysis of coupled THM processes in the near field is crucial for the understanding of the long-term behaviour of the barriers. The developed model uses generally available data from standard tests but attempts to incorporate special characteristics of the bentonite behaviour, let us mention the oversaturation, swelling and strong couplings of the processes. The model is implemented via COMSOL Multiphysics and validated by the simulation of THM processes which were monitored during operation of the FEBEX experiment and analysed during two dismantling phases of the experiment.

Keywords: modelling of coupled thermo-hydro-mechanical (THM) processes; specific aspects of THM processes in bentonite; oversaturation; implementation via COMSOL Multiphysics; analysis of the large scale FEBEX experiment

1. Introduction

The paper is motivated by the need for analysis of coupled thermo-hydro-mechanical (THM) processes which is necessary for the assessment of performance and safety of deep geological high-level radioactive waste storage facilities, see e.g. [1]. The need for coupled THM analysis is especially important for processes in the near field, close to the deposited canisters with the nuclear waste (the

spent nuclear fuel), i.e. in the bentonite-based sealing barriers and the surrounding host rock. This near field is in the initial stage of repository operation strongly influenced by the heat produced by the spent nuclear fuel; the bentonite barrier is slowly water-saturated from the surrounding (host) rock mass and influenced by the forces arising from swelling of the bentonite.

The processes in the host rock can be relatively well described by classical models for flow in porous media, but a special interest should be devoted to the modelling of the processes in bentonite barriers. This paper is devoted to the development of a reasonably simple THM model, which however considers the specific properties of the bentonite and provides the capability of simulation of THM processes in the bentonite sealing barriers. The specific features of the bentonite, as swelling and oversaturation induced by the complicated microstructure, will be taken into consideration. Moreover, these specific features will be described on the base of data from relatively standard laboratory tests. The capability of simulating the coupled processes will be demonstrated by simulation of processes occurring in the FEBEX experiment, i.e. Full-scale Engineered Barriers Experiment performed in the Grimsel test site in Switzerland.

Data available from monitoring THM processes during more than 18-year operation of the FEBEX experiment as well as the data from two phases of dismantling the experiment (after 5 and 18 years), will serve for validation of the described model. A selection of required data was available due to the participation in the international DECOVALEX project. The necessary data, as well as methodology for validation, were prepared by A. Gens, who was the coordinator of the relevant task of the project. The DECOVALEX project also offers the possibility of comparing the modelling technique described in this paper with modelling used by other teams with their approaches and different software, see [2], [3]. Note that modelling related to FEBEX experiment was also investigated in an earlier phase of the DECOVALEX project, see [4], [5].

Many papers provide a description of the FEBEX experiment and the material behaviour of the FEBEX bentonite and the granite host rock for the FEBEX experiment [6], [7], [8], [9], [10], [11], [12] and [13]. The development of mathematical models for the simulation of THM processes occurring during the experiment operation is described e.g. in [4], [5], [14], [15] and [16], the realisation of such models uses different software tools. The modelling, which was done during the phase DECOVALEX 2019 by using the software COMSOL Multiphysics, THAMES, TOUGH2+FLAC and HYDROGEOMECH, is described in [2], [3]. The model developed in this paper is implemented with the aid of COMSOL Multiphysics software, which provides enough tools and capabilities for simulation of complex coupled problems.

The specific aims of this paper are (1) treating of bentonite oversaturation by using the available data, (2) showing a significant influence of different expressions for vapour diffusion, (3) demonstration of the possibility of numerical implementation using the COMSOL Multiphysics

software, (4) simulation of THM processes during FEBEX experiment and comparison of the computed results with data from monitoring and dismantling.

The rest of the paper is organised as follows. Section 2 describes the basic principles for deriving separated THM models and their couplings which are considered in this paper. Section 3 is devoted to the explanation of oversaturation and swelling, construction of retention function suitable for FEBEX bentonite, discussion of the choice of the vapour diffusion coefficient and construction of other constitutive relations using the available data. Section 4 shortly describes the numerical implementation via COMSOL Multiphysics and the solvers offered there. The FEBEX experiment is briefly described in Section 5, the procedure of modelling the processes which occur in FEBEX in situ test is described in Section 6 including several phases of the test with changing geometry, necessary transfer of data between the following phases etc. Section 7 describes the outputs from the modelling and discusses the results, including the effect of different expressions for vapour diffusion and the correspondence with the measured data. The paper ends with general conclusions in Section 8.

2. Conservation equations and coupled THM model

This section aims to develop a THM model as simple as possible, but suitable for simulation of processes in bentonite sealing with various applications as it is demonstrated later in the paper. The focus is on the saturation and swelling of the bentonite which consists of solid part (s), liquid water (w), water vapour (v) and air (a). The pressure in gas (vapour and air) is assumed constant and consequently a Richards type, one-phase model is used for the description of flow in variably saturated bentonite. This section introduces the conservation equations for separate THM processes, then the interconnections among THM processes are mainly considered in Section 3. To keep the model relatively simple, we neglect some couplings which we consider weaker, not very significant. As general references for some details related to the provided description of the THM model, we can mention [17], [18] and also [19] and the references therein.

The model is described by equations which hold in the space-time domain $\Omega_t = \Omega \times (0, t_{max})$. For brevity of this section, we shall not discuss the boundary and initial conditions, but they must be included in the implementation of the model.

2.1 Water and vapour flow model

We consider a situation when water appears in two forms of liquid water and vapour. The mass conservation will be described by one equation (1), which can be derived as a sum of two mass

conservation equations for separate liquid water and vapour flow. If M_w and M_v denote the mass of water and vapour in a volume V, then the changes of M_w and M_v in time t can be expressed as

$$\frac{\partial M_w}{\partial t} = \int_V [-\nabla \cdot (\rho_w v_w) - E + Q_w] \, \mathrm{d}x,$$

$$\frac{\partial M_v}{\partial t} = \int_V [-\nabla \cdot q_v + E] \, \mathrm{d}x,$$

where ρ_w is the mass density of water, v_w is the Darcy velocity described later in (2), q_v is the diffusive mass flux of the vapour, see (5), and Q_w is the mass source term for water. In the considered model, Q_w is determined by the deformation and the level of water saturation of volume V, see Section 2.3. The term E denotes possible mass exchange between the liquid water and vapour, which in the sum disappears, see the classical paper [20]. Moreover,

$$\frac{\partial (M_w + M_v)}{\partial t} = \frac{\partial}{\partial t} \int_V (w\rho_d + m_v) \, \mathrm{d}x \approx \frac{\partial}{\partial t} \int_V w\rho_d \, \mathrm{d}x,$$

where w is the mass water content, ρ_d is the dry density and $w\rho_d$ expresses (density of) mass of the water. If M_w and M_s denote the mass of water and solid in the volume V, then $w = M_w/M_s$, $\rho_d = M_s/V$ and $w\rho_d = M_w/V$. The term $m_v = \rho_v \Phi_v$ stands for the mass of vapour, which can be expressed through ρ_v and Φ_v being the mass density and volume fraction for vapour, respectively. The mass density ρ_v can be expressed from the Kelvin-Laplace equation, see later in this subsection; the volume fraction Φ_v plays a role in the vapour diffusion, see Section 3.3. The term m_v can regularise the equation for w close to zero, which does not occur in the intended applications. Our simulations include the term m_v, but by numerical tests, it was found that neglecting this term just very slightly changes the solution.

Using the above equations, the mass conservation equation for the liquid water and vapour is considered in the following form

$$\frac{\partial}{\partial t}(w\rho_d) = -\nabla \cdot (\rho_w v_w + q_v) + Q_w. \tag{1}$$

The equation (1) represents a generalised Richards equation including non-isothermal vapour diffusion. A constant (atmospheric) gas pressure is assumed, $p_g = p_{atm} \approx 0$. This assumption corresponds with vapour transport only through diffusion and enables to formulate one-phase model without separate mass balance equation for the gas flow. For more details concerning the Richards equation, see e.g. [17]. The Richards and two-phase flow approaches are compared in [21].

In (1), v_w is the Darcy velocity

$$v_w = -\frac{k_s}{\mu} k_r(S_e) \nabla p_w, \tag{2}$$

where p_w is the pore water pressure, $p_w \geq 0$ and $p_w < 0$ for the water-saturated and unsaturated case, respectively, k_s is the (absolute, intrinsic) permeability in the fully saturated case, $k_r = k_r(S_e)$ is the relative permeability depending on the effective saturation with water S_e, μ is the dynamic viscosity of water.

We shall use definitions of the water saturation (S_w) and effective saturation (S_e) which are not related to volumes and porosity but which are expressed through the mass of water as follows

$$S_w = \frac{w}{w_{max}}, \qquad S_e = \frac{w - w_{res}}{w_{max} - w_{res}}, \tag{3}$$

where w_{max} and w_{res} are maximum and residual (minimum) water mass content. The definition of S_w and S_e given in (3) enables to include the oversaturation into the developed model. More detailed discussion on this topic and relation to saturation defined in a more usual way through (bulk) porosity is provided in the next section, see the equation (13).

Note that the saturated permeability is considered as depending on the dry density, $k_s = k_s(\rho_d)$, and through dry density also on the temperature, see Section 3.7. The dynamic viscosity also depends on the temperature T, $\mu = \mu(T)$. These topics are also discussed in the next section.

Assuming that w depends on p_w, ρ_d and T, the change of the water mass can be expressed as

$$\frac{\partial(w\rho_d)}{\partial t} = \rho_d \frac{\partial w}{\partial p_w}\frac{\partial p_w}{\partial t} + \rho_d \frac{\partial w}{\partial \rho_d}\frac{\partial \rho_d}{\partial t} + \rho_d \frac{\partial w}{\partial T}\frac{\partial T}{\partial t} + w\frac{\partial \rho_d}{\partial t}. \tag{4}$$

In the unsaturated case, the terms $\frac{\partial w}{\partial p_w}$, $\frac{\partial w}{\partial \rho_d}$ and $\frac{\partial w}{\partial T}$ can be computed from the definition of the retention function $w = f_r(p_w, \rho_d, T)$. The dependence of the retention function f_r on the pressure p_w (or suction $s = -p_w$), dry density and temperature will be discussed in Section 3.2. Note that ρ_d depends on the volumetric strain and temperature, therefore $\frac{\partial \rho_d}{\partial t} = \frac{\partial \rho_d}{\partial T}\frac{\partial T}{\partial t} + \frac{\partial \rho_d}{\partial \varepsilon_{el,v}}\frac{\partial \varepsilon_{el,v}}{\partial t}$, $\varepsilon_{el,v}$ is defined in Section 2.3 and more details can be found in Section 3.7.

Following [22], the vapour mass flux q_v can be primarily expressed as

$$q_v = -D_v \nabla \rho_v \,, \tag{5}$$

where the flux is driven by the gradient of the mass density of vapour and D_v is the diffusion coefficient. The vapour density ρ_v can be expressed from the Kelvin-Laplace equation

$$\rho_v = \varphi \rho_{vsat}(T), \qquad \varphi = \exp\left(\frac{p_w}{\rho_w r_v T}\right),$$

see e.g. [22] and [18], where φ is relative humidity, $\rho_{vsat}(T)$ is the density for full vapour saturation at the temperature T, $r_v = R/M_{mw}$ is the specific gas constant for water vapour, R is the universal gas constant and M_{mw} is the molecular weight of water. From the above formula, we get

$$\frac{\partial \rho_v}{\partial p_w} = \frac{\rho_v}{\rho_w r_v T}, \quad \frac{\partial \rho_v}{\partial T} = \varphi \frac{\partial \rho_{vsat}}{\partial T} - \frac{\rho_v p_w}{\rho_w r_v T^2} - \frac{\rho_v p_w}{\rho_w^2 r_v T} \frac{\partial \rho_w}{\partial T}.$$

Therefore, the diffusive mass flux of vapour can be expressed as follows

$$q_v = -D_v \left(\frac{\rho_v}{\rho_w r_v T} \nabla p_w + \eta \left(\varphi \frac{\partial \rho_{vsat}}{\partial T} - \frac{\rho_v p_w}{\rho_w r_v T^2} - \frac{\rho_v p_w}{\rho_w^2 r_v T} \frac{\partial \rho_w}{\partial T} \right) \nabla T \right). \tag{6}$$

Thus, the vapour mass flux has a part driven by the pore pressure gradient and a part driven by the temperature gradient. The determination of the diffusion coefficient is discussed in Section 3.3. Above, $\eta = 1$ gives the expression (5) and will be used in our model; $\eta > 1$ is a possibility (enhancement factor) introduced already in [22].

2.2. Heat transport

We shall assume that the heat propagation is solely done by the heat conduction; the heat from phase changes of water and the heat transport by convection are neglected. Therefore, the heat balance is described by the following equation,

$$c\rho \frac{\partial T}{\partial t} = \nabla \cdot (\lambda \nabla T) + Q_T, \tag{7}$$

where c is the heat capacity, ρ is the mass density, λ is the heat conduction coefficient and Q_T denotes the density of heat sources.

The heat capacity and the mass density in (7) concern the mixture of the solid matrix and water (contribution of the gaseous phase can be neglected), so that they are computed as averages of the corresponding quantities, i.e.

$$c = c_{s+w} = \frac{M_s c_s + M_w c_w}{M_s + M_w} = \frac{c_s + w c_w}{1 + w}, \quad \rho = \rho_{s+w} = \frac{M_s + M_w}{V} = \rho_d (1 + w),$$

where the already introduced notation is used.

2.3 Mechanics

The deformation of the porous body Ω is assumed to be described by the displacement u and the small strain tensor $\varepsilon = \varepsilon(u)$. Moreover, σ will denote the Cauchy stress tensor. The sign convention of continuum mechanics is used, i.e. expansive strains and tensile stresses are positive.

It is assumed that the triple (u, ε, σ) evolves in time in balance with the acting volume forces f. The time evolution of the system is due to time-dependent swelling and temperature changes. This

evolution is slow so that inertia forces can be neglected, and therefore the momentum conservation has the form

$$-\nabla \cdot \sigma(x,t) = f(x) \text{ for } (x,t) \in \Omega_t = \Omega \times (0, t_{max}). \quad (8)$$

We shall assume that the total stress has three components

$$\sigma = \sigma_{total} = \sigma_{effect} - \sigma_{water} - \sigma_{swell}\,, \quad (9)$$

where σ_{effect} is the (effective) stress related to elastic deformation of the solid matrix, σ_{water} is hydrostatic stress from the pore pressure and σ_{swell} is the stress due to swelling. The (total) strain is composed of two components:

$$\varepsilon = \varepsilon_{total} = \varepsilon(u) = \varepsilon_{el} + \varepsilon_{th}, \quad (10)$$

which are the elastic strain ε_{el} and the isotropic thermal expansion $\varepsilon_{th} = \frac{\alpha_v}{3}(T - T_{ref})I$. Here, α_v is the coefficient of volumetric thermal expansion, I is the unit tensor, T_{ref} is the reference (initial) temperature. Note that small strains are assumed, $\varepsilon = (\varepsilon_{ij})$, $\varepsilon_{ij} = (\frac{\partial u_i}{\partial x_j} + \frac{\partial u_j}{\partial x_i})/2$. Note that the volumetric parts of the strain tensors are defined through the trace, $\varepsilon_v = tr(\varepsilon) = \sum_i \varepsilon_{ii}$,

$$\varepsilon_v = tr(\varepsilon_{el}) + tr(\varepsilon_{th}) = \varepsilon_{el,v} + \varepsilon_{th,v}, \quad \varepsilon_{th,v} = \sum_i \varepsilon_{th,ii} = \alpha_v\big(T - T_{ref}\big).$$

Note also that the swelling is expressed through the stress.

We shall assume the strain-stress relation with the elastic tensor C,

$$\sigma_{effect}(x,t) = C(x,t) : \varepsilon_{el}(x,t), \quad (11)$$

where, in the case of isotropic material, the inverse relation to (11) can be described in the form

$$\varepsilon_{el,ij} = \frac{1+\nu}{E}\sigma_{ij} - \frac{\nu}{E}\sigma_{ef,v}\delta_{ij}, \quad \sigma_{ef,v} = \sum_i \sigma_{ii},$$

where $\sigma_{effect} = (\sigma_{ij})$, ε_{el}= ($\varepsilon_{el,ij}$), E is the elasticity modulus, ν is the Poisson ratio, $\sigma_{ef,v}$ denotes the volumetric component of the effective stress and δ is the Kronecker delta. In the case of some kinds of material nonlinearity, a variation of $C = C(x,t,\varepsilon(x,t))$ is admitted, see e.g. [23], [18]. Later in (24) and (25), we consider the evolution of elastic modulus in time, in dependence on dry density (involving strains) and suction (water saturation). We assume that plasticity effects can arise only as an effect of an increase of loading and therefore, the deformation theory of plasticity (materially nonlinear elasticity) is sufficient. Nevertheless, the model could be generalised for adopting loading/unloading behaviour by involving the Basic Barcelona Model (BBM) and its generalisation to non-isothermal states, see e.g. [24], [25].

The pore pressure contribution is as follows,

$$\sigma_{water} = \alpha \chi p_w I, \tag{12}$$

where α is the Biot-Willis constant, which is assumed to be equal to one in this paper, and χ is 'Bishop's function depending on the saturation. In the fully saturated case $\chi = 1$. In the unsaturated case, a standard $\chi(S_w) = S_w$, see [17], [18], is used for granite and concrete, but for the bentonite, we use $\chi = 0$, see e.g. [26]. Correspondingly, the source term $Q_w = \alpha \chi \frac{\partial \varepsilon_{el,v}}{\partial t}$, see also Section 3.7. The swelling stress σ_{swell} is described in the next section.

3. Constitutive relations and THM interactions

This section deals with the constitutive relations, which also describe the most significant couplings among the THM processes in the bentonite. Some more details can be found e.g. in [18] and [19].

3.1 Inner structure and specific properties of the bentonite

The term of oversaturation was already mentioned in Section 1 for the phenomenon that the bentonite is capable of storing more water than the amount corresponding to its standard (bulk) pore space $V_b = V - V_s$ where V_s is the volume of solid part within V. The corresponding porosity ϕ can be defined as

$$\phi = \frac{V - V_s}{V} = 1 - \frac{\rho_d}{\rho_s}.$$

The effect of oversaturation is a consequence of a complicated inner structure, see Fig. 1, and chemistry acting in the bentonite or, especially, in its component, the montmorillonite. The influence of this inner structure with (1) bulk pores, (2) interlayers and (3) double layers on the flow and diffusion could be explained by a triple porosity model with specific flow (diffusion) mechanism for each component – bulk pore water, interlayer water and double layer water with proper exchange rules for these water components. Also, chemistry, charges and ion system could be considered. For more details see e.g. [27], [28], [29] and the references therein. However, such description requires much knowledge, experimental data and research which is hardly available for the considered applications.

Therefore, we suggest to replace the quantities connected with porosity with quantities related to the mass of water like the water mass content w, see the definition of saturation (3). This definition of saturation avoids the necessity of analysis of more complicated pore structure and also the deformation of pores during the saturation process.

Using this idea, we construct a model using the available macroscopic data, which are, of course, affected by the mentioned inner structure. The saturation enters the model many times,

explicitly or implicitly, see the description of the retention function, the relative permeability, the vapour diffusion coefficient, the stress-strain relation and the swelling stress in the following subsections.

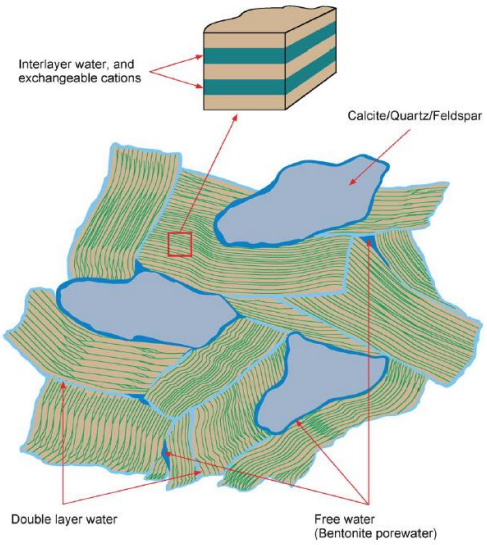

Fig. 1: Free (bulk) pore water, interlayer water and double layer water, see [30].

An important value w_{max} can be derived from the data provided for the construction of the retention function, see the next subsection. The accuracy of determination of w_{max} is influenced by the fact if data are available for the states close to full saturation (states with very low suction).

Note that many porous materials have less complicated inner structure and therefore can work with saturation S_r related to the bulk pore space and defined as follows

$$S_r = \frac{w}{w_{pore}}, \quad w_{pore} = \frac{\rho_w \phi}{\rho_d}, \quad S_r = \frac{w_{max}}{w_{pore}} S_w \geq S_w. \tag{13}$$

Above, the value w_{pore} corresponds to the full saturation of the bulk pores and obviously $w_{pore} \leq w_{max}$, but a sharp inequality is typical for the bentonite. The third identity in (13) provides a relation between S_r and S_w, which indicates that S_r can be greater than one. Values of $S_r > 1$ are confirmed by measurements, which can be seen e.g. in Fig. 5 and Fig. 13.

3.2 Retention function

We fit the data provided for the retention relation with a modified van Genuchten formula of the form

$$\mathrm{w} = f_r(s, \rho_d, T) = w_{max}(\rho_d, T) \cdot \left(1 + \left(\frac{s}{P_0(\rho_d)}\right)^{\frac{1}{1-\lambda_1}}\right)^{-\lambda_1} \cdot \left(1 - \frac{s}{P_{00}}\right)^{\lambda_0} \text{ for } 0 \leq s \leq P_{00}, \tag{14}$$

where λ_1, λ_0 are dimensionless parameters and P_0 , P_{00} are parameters expressed in MPa. P_{00} is the closing pressure, $s = p_g - p_w \approx -p_w$ is the suction in MPa. The suction s= 0 provides $w = w_{max}$, s= P_{00} provides $w = 0$. More precisely,

$$\begin{aligned} \mathrm{w} = f_r(s, \rho_d, T) = w_{max}(\rho_d, T) \text{ for full saturation } s \le 0, \\ \mathrm{w} = f_r(s, \rho_d, T) = w_{res} \approx 0 \text{ for } s > P_{00}. \end{aligned} \tag{15}$$

Note that w_{res}, appearing in the definition of the effective saturation (3), is assumed to be $w_{res} = 0.001 \approx 0$.

The expression (14) was fitted to the measured data for the FEBEX bentonite provided for different dry densities and different temperatures. It provides the following expression

$$w_{max}(\rho_d, T) = e^{-0.015\cdot(T-T_0)}\frac{{\rho_d}^3}{100} + \frac{\rho_w \phi}{\rho_d}, \quad P_0(\rho_d) = 10^{-5}\cdot e^{(8{,}2\cdot\rho_d)}, \quad P_{00} = 1000, \tag{16}$$

$\lambda_1 = 0.14$ and $\lambda_0 = 1.5$, the dry density and specific mass density of water are in the unit $\mathrm{Mg/m^3}$. The term $\rho_w\phi/\rho_d$ represents the mass water content in the bulk pores, see (13), $e^{-0.015\cdot(T-T_0)}{\rho_d}^3/100$ is an expression for the mass water content in extra pores, $T_0 = 20\,°\mathrm{C}$ is the initial (reference) temperature.

A comparison of the fitted expression (14) with (16) with experimental data can be seen in Fig. 2.

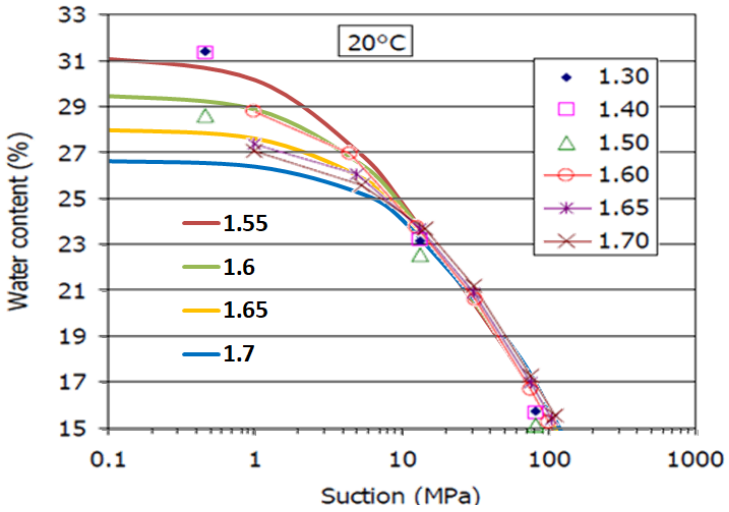

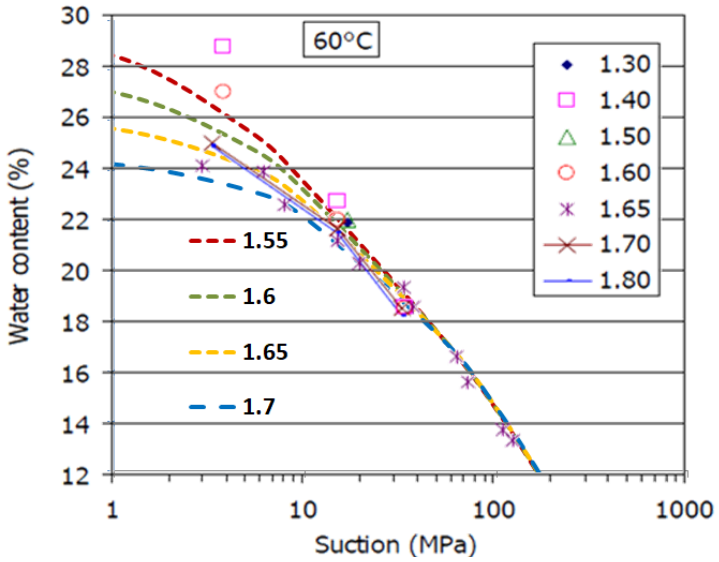

Fig. 2: Retention curves (bold and dashed lines) for different dry densities $\rho_d = 1.55;\ 1.6,;\ 1.65;\ 1.7\ \mathrm{Mg/m^3}$ (red, green, yellow and blue curves, respectively) and temperatures $T = 20, 60\ °C$ and a comparison with the measured data (isolated symbols) from [13].

Note that for the porous material like granite or concrete, the value w_{max} is fully determined by the bulk porosity ϕ, $w_{max} = w_{pore} = \rho_w \phi / \rho_d$, $\rho_w \approx 1\ Mg/m^3$. For w_{max} in bentonite, it is important to have water mass content measurements for saturation in the state of low suction.

The difference between w_{max} and w_{pore} in the bentonite can be balanced by introducing a higher mass density of the water $\rho_w^+ = \rho_w (w_{max}/w_{pore})$. Fig. 3 shows both the values ρ_w^+ derived from the experiments on the FEBEX bentonite and ρ_w^+ calculated from the expression (16) for w_{max}. In the case of experiments, the water density ρ_w^+ has been calculated from w_{max}, which was the final water mass content averaged over the whole tested samples. The correlation of both types of values provides additional evidence of the suitability of the expression of oversaturation given in (16).

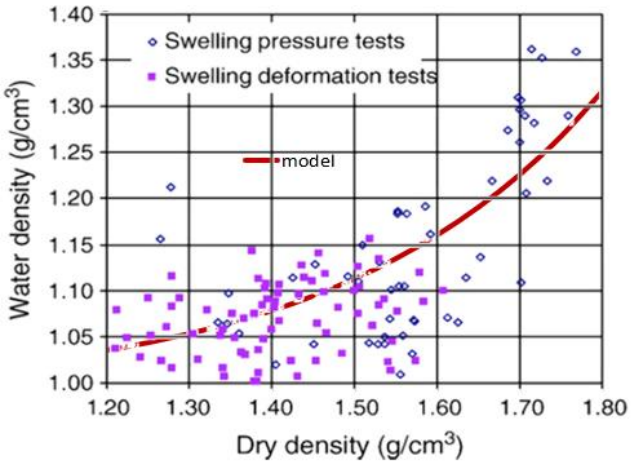

Fig. 3: Comparison of data derived from tests [31] (diamond and square symbols) and data derived from $\mathrm{w_{max}}(\rho_\mathrm{d}, \mathrm{T} = 20°\mathrm{C})$ defined in (16) (the red line in the picture).

3.3 Permeabilities and vapour diffusion

We assume that the saturated permeability depends on the dry density (similarly like w_{max}) and the following expressions (17) and (18) for the FEBEX bentonite were derived from the measured values [12],

$$k_s = k_s(\rho_d) = 6.46 \cdot 10^{-17} \cdot {\rho_d}^{-22.5} \ [\mathrm{m}^2], \tag{17}$$

$$k_s = k_s(\rho_d) = 2.0 \cdot 10^{-17} \cdot {\rho_d}^{-18.95} \ [\mathrm{m}^2], \tag{18}$$

see Fig. 4. The corresponding conductivities are computed through the standard formula $K_s = k_s g \rho_w / \mu$, where g is the gravitational acceleration and $\mu = \mu(T)$ is the dynamic viscosity of water, which depends on the temperature T, see e.g. [17]. Note that μ at $T = 20°$ is used for obtaining the graphs in Fig. 4.

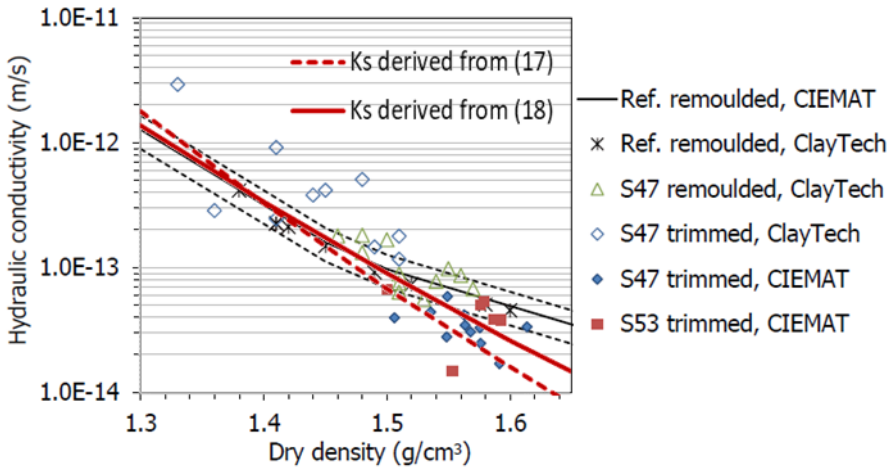

Fig. 4: Comparison of the hydraulic conductivities derived from the expressions (17) and (18) (see dashed and solid red lines) with measured data (isolated symbols).

The relative permeability depends on the effective saturation (3) and the following dependence is used for the FEBEX bentonite

$$k_r = k_r(S_e) = S_e^3, \tag{19}$$

The water vapour diffusion coefficient D_v, which appears in (5) and (6), should be determined experimentally, see e.g. [32], [33]. Generally, the expression for this coefficient has the form

$$D_v = 2.16 \cdot 10^{-5} \left(\frac{T}{273.15}\right)^{1.8} D_{vr}, \tag{20}$$

where the first part provides the diffusion coefficient through open air and D_{vr} is the relative diffusion coefficient depending on the air-filled porous space, see [33].

It can be assumed that $D_{vr} = c\phi(1 - S_w)$, where c is a proportionality factor and the expression $\phi(1 - S_w)$ stands for approximation of the volume fraction Φ_v, where the diffusion can occur. In this way, we shall consider

$$D_{vr} = \tau\phi(1 - S_w), \tag{21}$$

where τ is the tortuosity. The first choice is the value $\tau = 0.8$, which is used for the FEBEX bentonite e.g. in [34]. Another choice is the Penman-Millington-Quirk (PMQ) model

$$D_{vr} = 0.66\, \phi(1 - S_w)^2, \tag{22}$$

see [32]. It can also be interpreted as (21) with $\tau = 0.66(1 - S_w)$.

The above choices of τ are used in the definition of Model 1 and Model 2 in Section 6.2, and the application of these models in the modelling of FEBEX in situ test is discussed later in Section 7.

3.4 Heat

The heat conduction coefficient significantly depends on water saturation, i.e.

$$\lambda = \lambda(S_w).$$

The available data, see Fig. 5, show the dependency of λ on S_r, which is the relative saturation related to the bulk pore space defined in (13), see [4]. The dependence can be approximated by the expression

$$\lambda(S_r) = 1.28 - 0.71/\left(1 + e^{10\cdot(S_r - 0.65)}\right). \tag{23}$$

The dependence $\lambda = \lambda(S_w)$ is then obtained from (23) and the relation between S_r and S_w given in (13). The evaporation or condensation heat, see [19], is neglected in the developed THM model.

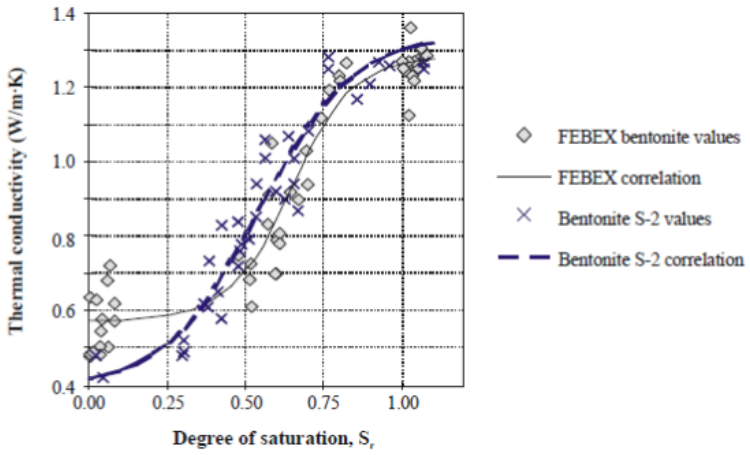

Fig. 5: Experimental data for FEBEX and S2 bentonites from [4]. FEBEX correlation (solid black line) corresponds to the formula (23).

3.5 Nonlinear elasticity

The elastic modulus is obtained from the oedometric experiments showing dependency of vertical (in this case also volumetric) strain ε_{vert} to the uniaxial (vertical) pressure (stress) σ_{vert}, see Fig. 6.

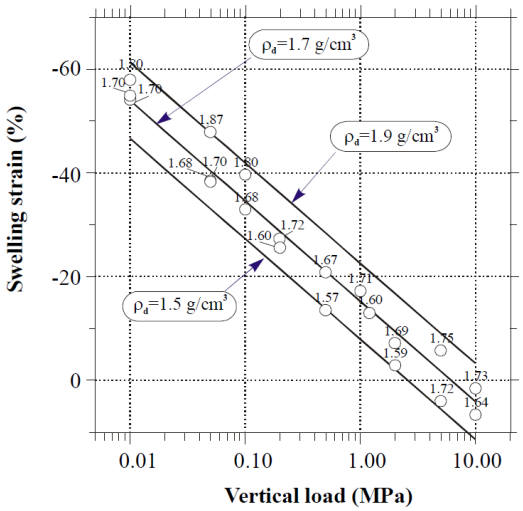

Fig. 6: Strains with elastic component for different vertical loads applied to fully saturated blocks with different values of initial dry density in $\mathrm{g/cm^3} = \mathrm{Mg/m^3}$, see [7].

The data from Fig. 6 are a summary obtained from a series of oedometric tests with cylindrical bentonite samples with different initial dry density, different external load, gradual saturation and swelling. The oedometric tests are assumed to be isothermal with laboratory temperature $T = 20°C$.

These oedometric tests can be simulated with hydro-mechanical model using the described relations plus information about the mechanical behaviour of bentonite. If isotropic behaviour is assumed and the Poisson ratio is estimated as $\nu = 0.3$, then we need to consider elastic modulus E depending on dry density, deformations and level of saturation.

With respect to the linear dependence of strains on the logarithm of the load, which is typical for soils, the elastic modulus for the saturated state is searched in the form of exponential dependence on dry density and strains. Because the dry density also depends on strains, the searched modulus can be expressed as depending only on dry density.

The inverse analysis of the data from oedometer tests, see Fig. 6, provides the relation

$$E_{sat} = E_{sat}(\rho_d) = \exp\left(8.2652\rho_d - 10.62\right) \text{ [MPa]}. \tag{24}$$

The above expression depends on the compaction expressed by the dry density ρ_d $[\mathrm{Mg/m^3}]$.

The dependence of elastic modulus on the level of saturation or equivalently on suction is studied e.g. in [35], and in the developed model it is simplified to the relation

$$E = E(s,\, \rho_d) = \begin{cases} E_{sat} & \text{if } s \le 0, \\ E_{sat} + \dfrac{s}{50}(E_{max} - E_{sat}) & \text{if } 0 < s \le 50 \text{ MPa}, \\ E_{max} & \text{if } s > 50 \text{ MPa}, \end{cases} \tag{25}$$

where s denotes suction in MPa, E_{sat} is defined in (24) and $E_{max} = 100$ MPa. This choice reflects the application in the analysis of FEBEX experiment with a significant number of gaps among blocks and the corresponding decrease of the dry density to $\rho_d = 1.6\ \mathrm{Mg/m^3}$ (in FEBEX the dry density of isolated block is $\rho_d = 1.7\ \mathrm{Mg/m^3}$).

3.6 Swelling

The effect of swelling is again a consequence of the inner microstructure of the bentonite. We use the expression

$$\sigma_{swell} = \sigma_{swell}(w, \rho_d) = \frac{w - w_{init}}{w_{max} - w_{init}} \sigma_{swell,max}\, I, \tag{26}$$

where w_{max} is taken from (16), w_{init} is the water mass content in the time when we start to consider swelling stress and $\sigma_{swell,max}$ depends on the dry density ρ_d expressed in $\mathrm{Mg/m^3}$ and was determined from the fitting of experimental data from [7] as

$$\sigma_{swell,max} = \sigma_{swell,max}(\rho_d) = \exp(6.77\rho_d - 9.07)\ [MPa]. \quad (27)$$

3.7 THM induced changes of the densities and the pore space

Let us assume that the solid grains, which occupy the volume V_s, are relatively stiff so that their mechanical deformation is negligible. On the other hand, the thermal expansion of the solid is not neglected. Then the mass density $\rho_s = \rho_s(T)$ and the volumetric thermal expansion coefficient $\alpha_v = \alpha_{vs}$ can be expressed as

$$\alpha_{vs} = \frac{1}{V_s}\frac{\partial V_s}{\partial T} = -\frac{1}{\rho_s}\frac{\partial \rho_s}{\partial T}.$$

Integration of this differential equation with the initial condition $\rho_s(T_{ref}) = \rho_{s0}$ then provides

$$\rho_s = \rho_s(T) = \rho_{s0}\, e^{-\alpha_{vs}(T-T_{ref})}. \quad (28)$$

Similarly, assuming incompressibility of water,

$$\rho_w = \rho_w(T) = \rho_{w0}\, e^{-\alpha_{vw}(T-T_{ref})}, \quad (29)$$

but here α_{vw} still depends on the temperature.

Under the assumption of stiff solid grains and correspondingly the Biot-Willis coefficient $\alpha = 1$, the change of porosity ϕ can be expressed by the following differential equation derived from the mass balance of the solid component under the small strain assumption

$$\frac{\partial \phi}{\partial t} = (1-\phi)\left(\frac{\partial \varepsilon_v}{\partial t} - \alpha_{vs}\frac{\partial T}{\partial t}\right) = (1-\phi)\frac{\partial \varepsilon_{el,v}}{\partial t}, \quad (30)$$

where $\varepsilon_v = tr(\varepsilon)$ and $\varepsilon_{el,v} = tr(\varepsilon_{el})$. For more details, see e.g. [19].

The solution of the equation (30) has the form

$$\phi(t) = 1 - (1-\phi_0)\exp(\varepsilon_{el,v,0} - \varepsilon_{el,v}(t)), \quad (31)$$

where ϕ_0 and $\varepsilon_{el,v,0}$ describe an initial state. The use of a simple Padé approximation $e^x \approx \frac{1}{1-x}$ provides an approximate expression used in the implementation

$$\phi \approx \frac{\phi_0 + \varepsilon_{el,v} - \varepsilon_{el,v,0}}{1 + \varepsilon_{el,v} - \varepsilon_{el,v,0}}. \quad (32)$$

Finally, note that $\rho_d = \rho_s(1-\phi)$ depends on temperature and the volumetric strain $\varepsilon_{el,v}$.

4. Numerical solution and implementation

The model is implemented via the finite element software COMSOL Multiphysics [36]. The thermal and hydraulic parts of the model are implemented in PDE (partial differential equation) module. It was necessary due to complicated links including thermal vapour term in the Richards equation. For axisymmetric model, the transformation into cylindrical coordinates should be additionally implemented as the PDE module directly offers only Cartesian coordinates. The mechanical part is implemented via the Structural mechanics module.

Two of the basic equations describing THM processes, namely heat conduction and Richards equation, are treated as strongly coupled and involve time derivative of the basic unknowns. The momentum balance equation does not involve the time derivative of the displacement (no inertia forces); displacements just instantly react to changes of loading.

The space discretisation is done through weak formulation and the finite element (FEM) method. A locally refined mesh of finite elements is used for all THM processes, see Fig. 8. Finite elements with quadratic polynomials are used for discretisation of heat and fluid flow, finite elements with cubic polynomials are used for the analysis of stresses and strains. The time discretisation uses the backward Euler method, which leads to a time-stepping procedure with the requirement of solving complex nonlinear system in each time step. This system arises from the finite element discretisation of all coupled THM processes, i.e. thermal-hydraulic and mechanical parts.

COMSOL Multiphysics offers two tools for solving the system, monolithic (full coupled) and segregated solvers as well as their combinations, see [36]. So, the segregation is used between mechanical part and thermal-hydraulic part, and a monolithic damped Newton solver treats the thermal-hydraulic part. The adaptive time step control watches both discretisation error and convergence of the solver for the systems arising within the time steps.

COMSOL Multiphysics allows to abstract from details of the implementation of numerical methods and considers it as a black box. Thus, we can only mention that the default accuracy was used during the computations. Some difficulties with the convergence arose in the case of inconsistent boundary and initial conditions which occur e.g. during the transition from one modelling phase of the FEBEX experiment to another one with possibly changed geometry. To overcome such convergence problems very short artificial transition phases were used.

5. The FEBEX in situ test

The full-scale engineered barriers experiment (FEBEX) was a research and demonstration project that was initiated by the "Spanish Agency for Radioactive Waste Disposal" (ENRESA). It followed from the

Spanish concept for the isolation of high-level radioactive waste. The subject of study in this article is the FEBEX in situ test, which was located in a crystalline host rock of the Aare Massif in central Switzerland in the Grimsel Test Site [9].

The primary goal of the FEBEX test was to study the behaviour of near-field components in a repository for high-level radioactive waste in granite formations, demonstration of the feasibility of constructing the engineered barrier system in a horizontal configuration, and analysis of the technical problems of this type of disposal method. The secondary aim was to develop modelling tools for the thermo-hydro-mechanical (THM) and thermo-hydrogeochemical (THG) processes and provide validation of models against experimental results [9].

The FEBEX in situ test involves the installation of two cylindrical heaters (4.54 m long and 0.9 m in diameter) disposed in a cylindrical steel liner with holes (diameter 0.97 m) centred in a tunnel (diameter 2.27 m) excavated by TBM (a tunnel boring machine). The rest of the space was filled by a barrier (thickness 0.64 m) made of highly compacted unsaturated blocks of the FEBEX bentonite. The backfilled area was sealed with a plain concrete plug placed into a recess excavated in the rock and having a length of 2.70 m (Fig. 7).

A total of 632 instruments were placed in the host rock and buffer to monitor relevant values of temperature, humidity, total and pore pressure, and displacements. A more detailed description of the spatial dimensions, bentonite placement, sensor placement, and experiment installation is provided in [6].

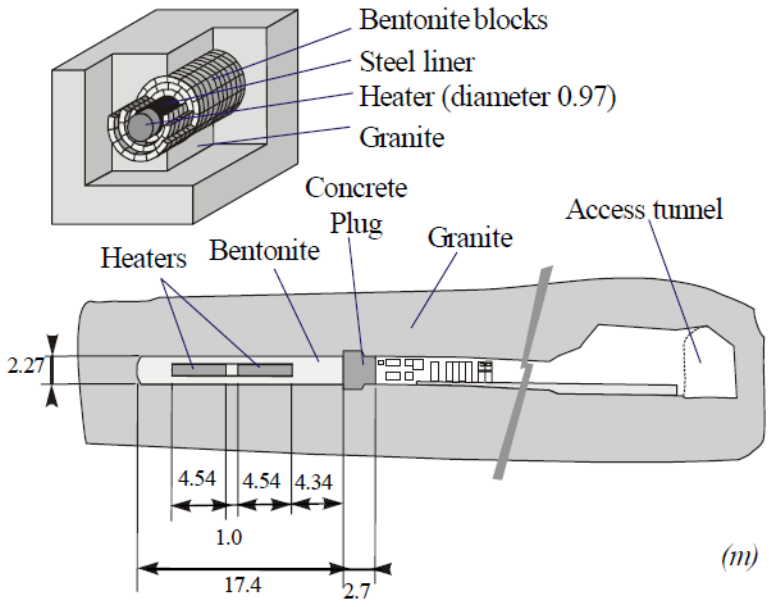

Fig. 7: The FEBEX experiment.

The FEBEX project started in 1994. One year later started the FEBEX in situ test with rock-mass characterisation and tunnel excavation. The construction of the concrete plug was completed in October 1996, and the heating began on February 27, 1997. The power of heaters was first increased stepwise and manually to reach a targeted maximum heater temperature of 100 °C for 53 days. After that, the system was switched to automatic mode for keeping the constant temperature at 100 °C in one measurement point in the middle of each heater [9].

Partial dismantling of the concrete plug and buffer around the heater closer to the access tunnel was carried out during the summer of 2002, after five years of continuous heating. The removed area was up to a distance of 2 meters from the second heater to minimise disturbance of the non-dismantled area. During this dismantling process, the second heater stayed operational. Afterwards, additional sensors were installed and a steel cylinder with a length of 1 m was inserted in the void left by the removed heater in the centre of the buffer, and the experiment was again sealed. All details of the dismantling process and measurements of dismantled data are described in [8].

The second heater stayed operational for 18.4 years and the rest of the FEBEX test was dismantled in 2015, including the second heater. A number of parts of the FEBEX test were studied, like bentonite, rock, relevant interfaces, sensors, metallic components, and tracers. Detail description of the second dismantling process is in [11]. The monitoring data from the FEBEX in situ test are evaluated in [37], and the final report from the dismantling of the FEBEX test is provided in [11].

6. Numerical model of the FEBEX experiment

Due to the horizontal deposition of heaters and axisymmetric geometry of the experiment, the model of the FEBEX experiment is treated as 2D-axisymmetric with axis placed in the middle of the circular tunnel with heaters. This axisymmetric simplification is natural for the saturation and heat flow and acceptable for the mechanics with swelling dominating over gravitational forces and the effect of possibly anisotropic initial stress. The cross-section shown in Fig. 8 has 50 m in radial and 120 m in axial directions, see Figs. 8 and 9. These dimensions are supposed as sufficient; the model does not show a change of temperature against initial temperature for 18.4 years at the outer boundary of the computational domain. The finite element mesh is depicted in Fig. 8. Quadratic finite elements are used for space discretisation of heat and water flow, and cubic elements are used for the mechanical part. The mesh for space discretisation includes 8 659 triangular and 3 736 quadrilateral elements, i.e., in total maximum of 12 395 elements. The number of elements depends on the modelling phases, see Section 6.2.

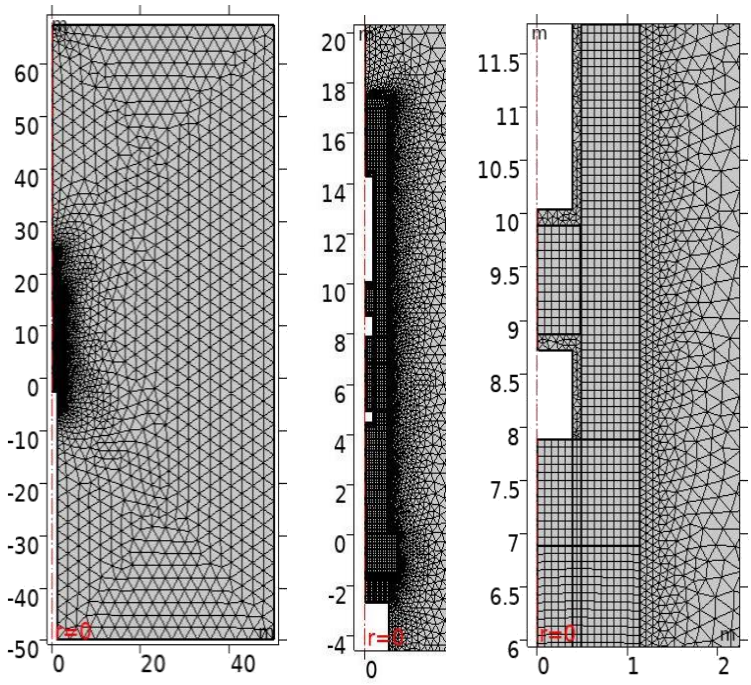

Fig. 8*:* Finite element meshes – the whole computational domains and the details.

The computational domain is divided into five subdomains, see Fig. 9, where each subdomain represents the same type of material. Most of the material properties and initial conditions used in the developed THM models are summarised in Table 1. In more details, the initial conditions for each subdomain are as follows.

Crystalline host rock has initial water pressure $p_w = 0.7\ \mathrm{MPa}$ and isotropic horizontal initial stress 28 MPa. Bentonite blocks have initial dry density $\rho_d = 1.6\ \mathrm{Mg/m^3}$. This value corresponds to the average between compacted blocks of FEBEX bentonite with initial $\rho_d = 1.7\ \mathrm{Mg/m^3}$ and technological gaps. The initial water content of bentonite blocks is $w_{init} = 0.14$. The corresponding suction is 135 MPa. Concrete plugs (original and second one constructed after the first dismantling) have initial suction 10 MPa. The initial temperature in all subdomains is 12 °C.

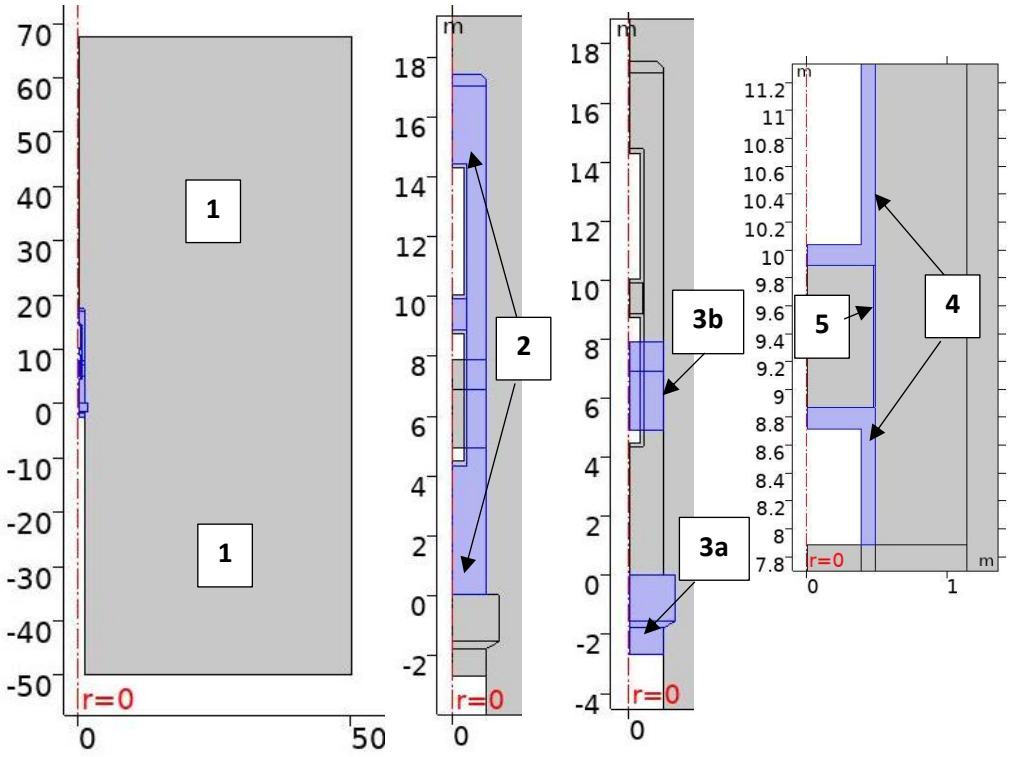

Fig. 9*:* Computational domains. 1. Crystalline host rock, 2. Bentonite, 3a. Original concrete plug, 3b. New concrete plug, 4. Heater, 5. Liner.

Table 1: Material properties. Identifiers (a)-(e) refer to notes given below the table.

	bentonite	**rock**	**concrete**	**heater TM**	**liner**
Initial dry density ρ_d [Mg/m^3]	1.60 (a)	2.64	2.2	7.8	7.8
Initial porosity ϕ [-]	0.41	0.016	0.11 (b)	-	*0.1*
Initial pressure p_w [MPa]	-135	0.7	-10	-	-135
Saturated permeability k_s [m^2]	(17), (18)	$5 \cdot 10^{-18}$	$5.7 \cdot 10^{-20}$(b)	-	$4 \cdot 10^{-21}$
Relative permeability $k_r = S_e^n$,	*n*=3	*n*=1	*n*=8	-	*n=1*
w_{max} [kg/kg$_{bentonite}$]	(16)	=ϕ/ρ_d (c)	=ϕ/ρ_d (c)	-	=ϕ/ρ_d
w_{res} [kg/kg$_{bentonite}$]	0.001	0.0001	0.001	-	0.001
λ_1 van Genuchten [-]	0.14	0.595 (d)	0.404 (b)	-	0.17 (e)
P_0 [MPa]	(16)	1.74 (d)	13.1 (b)	-	4.5 (e)
λ_0 van Genuchten [-]	1.5	-	-	-	-
P_{00} [MPa]	1000	-	-	-	-
Elastic modulus E [GPa]	(24), (25)	60	30	210	210
Poisson ratio ν [-]	0.3	0.25	0.3	0.3	0.3
Thermal conduct. λ [Wm^{-1}K^{-1}]	(23)	3.6	1.7	46	46
Linear thermal expansion α_{vs} [-]	10^{-5}	$7.8 \cdot 10^{-6}$	10^{-5}	10^{-5}	10^{-5}

Tortuosity τ [-] for Model 1	0.8	1.0	1.0	-	1.0
Tortuosity τ [-] for Model 2	$0.66(1-S_w)$	1.0	1.0	-	1.0

Labelled notes to the data in Table 1:

(a) Average value considering the dry density of blocks and the presence of gaps. (b) According to [38]. (c) Maximal water content fully determined by the (bulk) pore space. (d) Retention function from [15] for Grimsel granite. (e) Retention function from [15] for bentonite with dry density 1.58-1.59 $\mathrm{Mg/m^3}$.

Further comments on the data in Table 1:

THM model described in Sections 2 and 3 is considered for all materials with the exception of the heater. For the heater, a thermo-mechanical behaviour is assumed. A simplification is used for rock and concrete, where a classical retention function depending only on suction and without the closing term is used. All other parameters are kept constant. The liner is supposed to have thermo-mechanical properties as steel, but due to the holes, the flow through liner is possible. Therefore, THM model is also used for the liner with modified parameters.

6.1 Computational phases

The FEBEX experiment evolves in time, and consequently, different phases must be considered in the modelling. FEBEX experiment formally started 25/09/1995 by tunnel excavation and ended 20/07/2015 by the end of the final dismantling. The computational phases are described in detail in [9] as well as in [2] and [3]. It is essential to realise that the computational domain changes in time, e.g. by removing a part of the domain after the first dismantling or by the construction of the second plug.

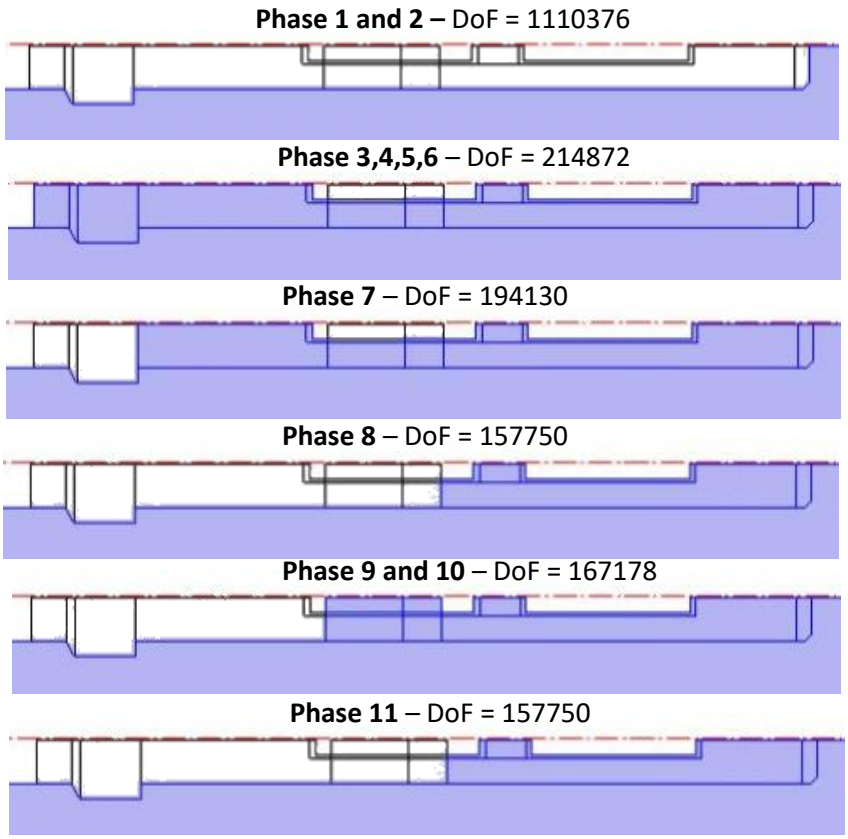

Fig. 10 Computational phases with different degrees of freedom (DoF) – active DoFs are inside the coloured parts of the model.

The numerical model is divided into 11 phases, which follow each other, see Fig. 10. The boundary conditions and occasionally the computational domain change for each phase. The primary aim is to model the whole lifetime of the FEBEX test to mirror all major changes in the computational domain.

Phase 1 (35 days) represents the excavation process. Phase 2 (300 days) is the ventilation period. It ensures some desaturation of the rock in the vicinity of the deposition borehole. Both phases are necessary for the preparation of host rock conditions before the installation of the experiment. The boundary conditions for both phases are as follows: (a) temperature 12 °C, suction 0 MPa for Phase 1 and 20 MPa (relative humidity RH 85%) for Phase 2 and zero normal stress on the borehole wall; (b) temperature 12 °C, water pressure 0.7 MPa, mechanical pressure 28 MPa on the outer part of boundary parallel with the borehole wall; (c) no flow and zero normal displacements are prescribed on the rest of the boundary. The geometry of the computational domain can be seen in Fig. 10.

Phase 3 (135 days) changes the geometry of the model and represents the installation of all components – bentonite barrier, heaters, concrete plug and liner. Bentonite gradually starts to saturate, and stress grows in this phase. The initial state is taken from the previous phase. Connections between THM processes in different subdomains are established by interface conditions.

Phases 4 (53 days), 5 (1773 days) and 6 (89 days) represent different stages of heating. During Phase 4, constant values of power were set for both heaters. At first, 1 200 W for 20 days and then 2 000 W for 33 days were set for both heaters. Phase 5 is a long heating period in which heat output was set such that the temperature of 100°C is kept in the sensors located in the middle of the length of each heater. This setting was also simulated within the computational model. During Phase 5, the power of the heaters is firstly transformed into constant heat flux over the surface of heaters, then the power of the heaters is computed to give the temperature 100°C in the position of sensors. The computation of the corresponding power of the heater is done through the tool of COMSOL Multiphysics (implementation of constraint). The course of the temperature along the length of the heater is shown in Fig. 11. Phase 6 represents the cooling period which occurs after the turning off the heater closer to the access tunnel. In this phase, the adiabatic (zero heat flow) boundary condition is imposed on the whole boundary of the turned-off heater.

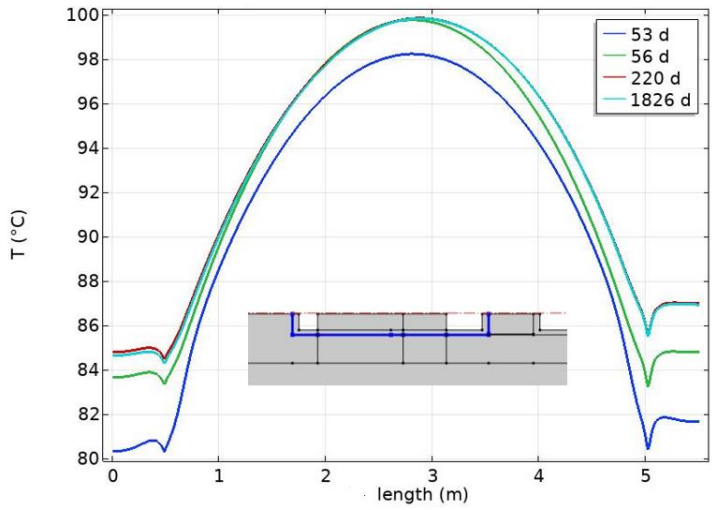

Fig. 11: Calculated temperature along the heater length on the outer shell of the heater closer to the access tunnel.

Phase 7 (51 days) starts with the removal of the original concrete plug and at the end of this period, the first dismantling data, concerning the removed bentonite, are obtained. Original zero normal stress condition was returned on the deposition borehole wall instead of the original contact of the concrete plug and the granite. On the interface of the bentonite and the original concrete plug - temperature 12°C, no flow, and zero normal stress were prescribed [8]. Phase 8 (4 days) started immediately after Phase 7 and represents the construction of the new plug. The comparison of the model results against the data from the dismantling process is shown in the next section.

Phase 9 (4660 days) begins after the installation of a new concrete plug for protecting further swelling of the bentonite. The main role of this phase is long natural hydration for nearly 13 years under the control of the maximum heater temperature.

Phase 10 (14 days) is the period of cooling the FEBEX test after turning off the second heater. In this phase zero heat flow is prescribed on the whole boundary of the second heater.

Phase 11 (114 days) starts with removing of the second plug [11]. Data from the second dismantling process [12] are obtained at the end of this phase. A comparison of the model outputs against the dismantling data is provided in the next section, see also [2] and [3].

The simulation of the FEBEX in situ test included all eleven phases. The modelling results consider mainly two stages, the first one considers outputs after performing Phases 1 to 8, the second one after Phases 8 to 11. The detailed description of all settings is in [2] (Annex F).

6.2 Variants of the THM model for bentonite

The modelling of the processes in FEBEX bentonite was performed by two THM models which use the relations and data described in Sections 2 and 3, and parameters described in Table 1. The models differ only slightly in the adopted expressions for saturated permeability. The main difference is in the choice of expression for vapour diffusion. As we shall see in the next section, this difference in model setting can lead to a more significant difference in some outputs. The differences in the variants of the model are just the following.

Model 1 uses the saturated permeability (18) and the relative vapour diffusion coefficient using the formula (21) with the tortuosity $\tau = 0.8$. Model 2 uses the saturated permeability (17) and the relative vapour diffusion coefficient using the formula (22).

Note that the outputs from Model 1 are similar as outputs presented in [15] for the first five-year period, where outputs from this model fit very well the measured data from the first dismantling (dry density and water content). Model 1 was consequently used for modelling the saturation up to the final dismantling. But then it provided a significantly lower value of the mass water content than shown by the experimental data, see Fig. 13. Similar observations are presented in a blind study provided within [16] with modelling performed by the CIMNE (International Center for Numerical Methods in Engineering, Spain) using the CodeBright software.

This inconsistency between the model outputs and measured data in the water content motivated searching for possible reason and change of Model 1. As the model results provide a good agreement with in situ data after first dismantling, a simple change of parameters was not acceptable. A suitable change was found in the modification of the vapour diffusion coefficient, which played a significant role in the saturation, especially in locations close to heaters. Therefore, the Penman-Millington – Quirk (PMQ) model, see [32], was adopted and used in Model 2. The hydraulic

permeability should be slightly decreased to fit the data after the first dismantling. A further discussion concerning the introduced models can be found in the next section.

7. Comparison of computed results with experimental data

This section describes the simulation of the THM processes in the bentonite barrier during the operation of the FEBEX in situ test. The simulation follows all phases described in the previous section and uses the mathematical model described in Sections 2 and 3 with two model variants (Model 1 and 2) which differ mainly in the adopted vapour diffusion term.

Some outputs were selected which characterise the fitting of computed values with experimental data in different space positions (different cross-sections and different distances from heaters) with time evolution to 5 years (about 1800 days) and 18 years (about 6600 days). The outputs also characterise sensitivity to some relations included in the model. Note that more outputs are presented in [2].

Fig. 12 shows the comparison of experimental data from the monitoring of time evolution of temperatures, relative humidity and total radial and axial stress against computed results using both models 1 and 2. The main difference between the models 1 and 2 can be seen in the time evolution of the humidity. Both models fit this evolution for five years. For the evolution up to 18 years, there is less high-quality experimental data, especially for the relative humidity close to the remaining heater. Thus, it is more difficult to evaluate the fit of the models, but the difference between the results provided by the models 1 and 2 is significant. A better comparison of the models is possible if the data from dismantling are considered, see Fig. 13.

Note that the measurement data in Fig. 12 also show some difference between measurements from different sensors in the same cross-sections. These differences show some heterogeneity and the difficulty of the measurements. As concerns the fit of radial stresses, note that real measurements were provided by pressure sensors placed into gaps between bentonite blocks and therefore they indicate real stress only after some time necessary for filling the gaps by swelling. Further, there was an asymmetric gap between the rock and bentonite at the top of the tunnel. This gap also had to be closed prior to accurate measurements. These construction facts, as well as asymmetric gravity forces, are not included in the model. Obviously, the model then gives an immediate increase of stresses. Also, the use of elasto-plastic behaviour for the bentonite could increase the accuracy of the model.

The comparison of computed data with data from dismantling after 5 and 18.4 years of experiment operation is depicted in Fig. 13. This figure focuses on the areas of two cross-sections passing through the middle of heaters with high-temperature gradients, where the thermal vapour

diffusion plays a significant role. The comparison shows that both Models 1 and 2 are comparable and provide a good fit for dismantling after five years, but the Model 2 is better in fitting the experimental data from dismantling after 18.4 years, especially in water content and degree of saturation.

The obtained results suggest a question of how further optimise the relations and parameters in THM model. One possibility is e.g. 3D model; another possibility is the introduction of heterogeneity, namely the use of different parameter settings in different parts of the computational domain. This requires to get more input information, but otherwise, the model will not be able to be accurate in some aspects. This is illustrated below.

The graph in Fig. 14 shows the power of both heaters recorded during the experiment operation [39]. In the first five-year period both heaters were active and the power of both was controlled by temperature sensors to be 100°C in the middle of the heater length. The available information about the FEBEX test does not indicate any source of difference in the heat power between both heaters as they should be surrounded by the same arrangement of bentonite blocks and surrounded by the same granitic rock, the water supply at the bentonite-granite interface should be sufficient, see [15].

However, in the experiment, there is about a 10% difference in the power of heaters. The power is lower for heater #1 located in the rear part of the FEBEX experiment, which was dismantled first, after five years of operation. It indicates that some difference (heterogeneity) in physical reality should exist. The different heat power of heaters can be explained by different heat dissipation due to higher water saturation around the heaters. Such a situation could be caused by higher permeability of the bentonite block around heater #2 or slower closing of technical gaps between the bentonite blocks and therefore better water conduction and faster bentonite saturation than in the vicinity of the first heater. Logically, without introducing some heterogeneity, the model is not able to explain this effect.

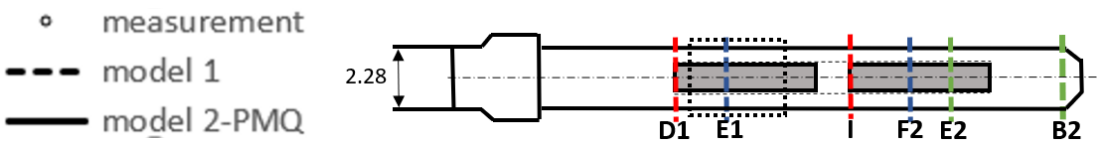

Temperature, section D1, 5 years of evolution **Temperature, section I, 18 years of evolution**

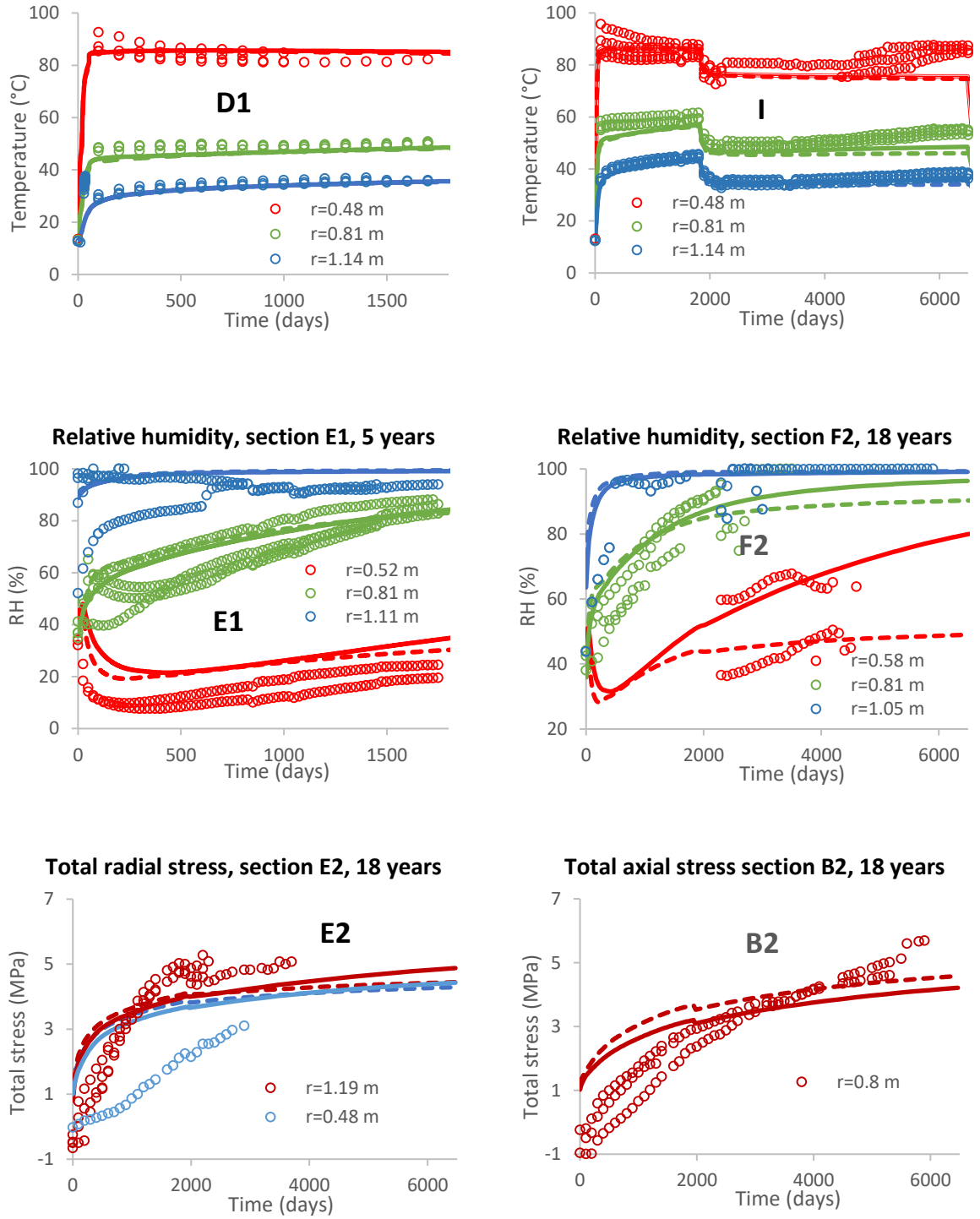

Fig. 12: Comparison of time-dependent evolution up to 5 and 18 years of measured and calculated values of temperature, relative humidity and total radial and axial stress in selected cross-sections and distances from the heaters. Circles denote measurements by several sensors in each cross-section, dashed and solid lines show output from Model 1 and Model 2, respectively. Colours indicate different distances from the tunnel axis. Note that positive stress in this figure means compression.

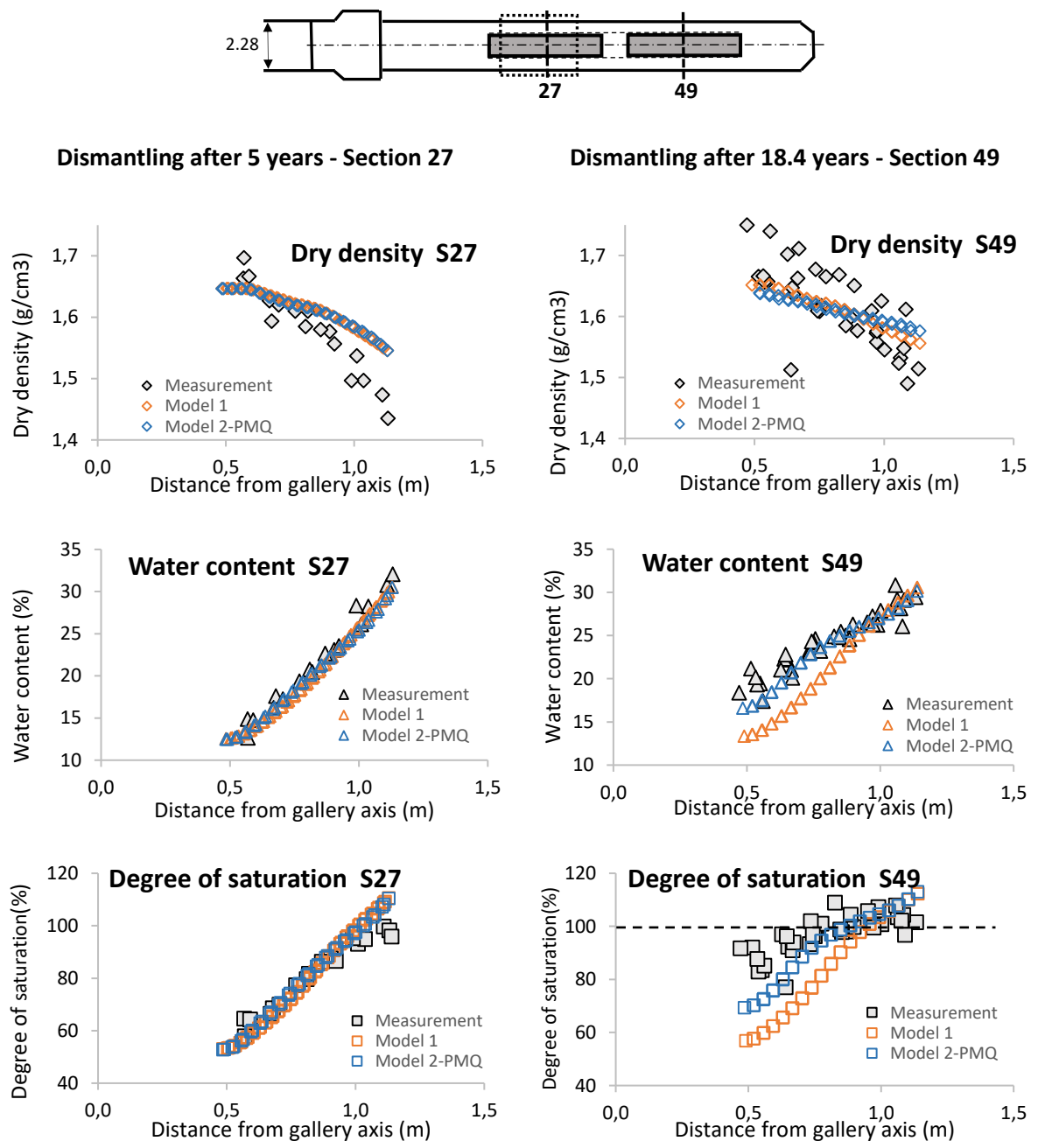

Fig. 13: Comparison of measured and calculated values of dry density, water mass content and degree of saturation in the area with a large temperature gradient (sections 27 and 49 through the heaters). Comparison with data from the first partial dismantling (5 years) and the complete dismantling (18.4 years) of the experiment. The description of the saturation uses the definition related to bulk pores (13) and corresponds to the state after dismantling. Consequently, the saturation goes over 100% (oversaturation occurs).

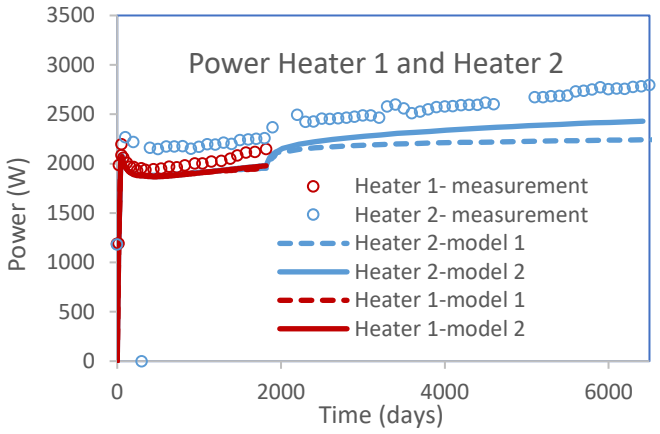

Fig. 14: Measured and computed power of the heaters (Heater 1 is closer to the access tunnel), see [39].

8. Conclusions

This paper formulates a model and its variants suitable for simulation of the THM processes occurring in the bentonite barriers around canisters with the spent nuclear fuel in a deep geological repository and similar applications. The main focus is on the processes in bentonite including the special character of bentonite behaviour with oversaturation and swelling.

The introduced THM model includes (1) flow in a variably saturated bentonite described by Richards type equation with vapour diffusion, (2) nonlinear elasticity and (3) heat propagation by conduction. A novelty of the model is the introduction of saturation which is not related to filling the pores but described by using the ratio of the current and maximal mass water content. This definition allows to include the oversaturation effect, which was measured in FEBEX in situ test. Subsequently, the model uses the water retention function providing the relation between the mass water content on one side and the suction, dry density and temperature on the second side. Such dependence is approximated by a modified multivariable van Genuchten function which includes the oversaturation term and fits reasonably well the provided measurement data. Special care is also devoted to vapour diffusion, which has a significant role in the model, as it was shown in the previous section.

Implementation of the model with proper discretisation in space and time and solvers for coupled multiphysics, including nonlinear processes, is a challenging task that was successfully done by using the tools provided by COMSOL Multiphysics software. Still, some effort in further development will be required in the future to fully control the discretisation error and enable the efficient solution to problems in 3D space (in the modelling of the FEBEX experiment with horizontal deposition of the heaters, it was natural to use the 2D axisymmetric simplification of the situation).

The introduced THM model was used for the simulation of THM processes occurring in the FEBEX in situ test. We can finally conclude the following.

The performed simulations used high-quality data available for the FEBEX bentonite behaviour obtained from careful laboratory testing. The availability of such data is crucial for the model application.

It was demonstrated that the introduced THM model and its implementation can provide the simulation of the processes occurring in FEBEX in situ test with the results which are in a good agreement with the experimental data or trends visible from the experimental data. In such a way, the FEBEX in situ test provided a validation of the model and its implementation.

The reported results show the significance of the role of some relations and parameters in the model. We can mention the expression of saturation and retention function through water mass content and maximum water content higher than just filling of bulk pores (oversaturation); modelling THM processes with specific parameters, which are evolving in time and depend on the current state of all processes; the significance of finding a proper expression for the vapour diffusion, which is suitable for the regions close to heat sources and simulation over longer time periods.

It was shown that the application of the model could encounter some uncertainties in the description of the situation, e.g. uncertainties induced by the heterogeneity of the geological environment and the barrier itself (see the discussion about the different power of the heaters in the previous section). Such uncertainty should be studied and estimated by simulations under different conditions and heterogeneities of the environment.

The FEBEX in situ test provides unique and high-quality data, which enables the development of proper mathematical models involving coupled THM processes and validation of such models against the experimental data. It also enables comparison of different approaches to construction and implementation of the models, see [2] and [3]. This paper would like to contribute to the core idea of the DECOVALEX project which says that the combination of experiments and modelling is the way how to get the knowledge necessary for understanding processes which are crucial for the construction of a safe deep geological repository of the high-level radioactive waste.

Acknowledgement:

DECOVALEX is an international research project comprising participants from industry, government and academia, focusing on development of understanding, models and codes in complex coupled problems in sub-surface geological and engineering applications; DECOVALEX-2019 is the current phase of the project.

The authors appreciate and thank the DECOVALEX-2019 Funding Organisations Andra, BGR/UFZ, CNSC, US DOE, ENSI, JAEA, IRSN, KAERI, NWMO, RWM, SÚRAO, SSM and Taipower for their financial and technical support of the work described in this paper. The statements made in the paper are, however, solely those of the authors and do not necessarily reflect those of the Funding Organisations.

References

[1] Pusch R. Geological Storage of Highly Radioactive Waste. Current Concepts and Plans for Radioactive Waste Disposal. Springer; 2008.

[2] Gens A, Alcoverro J, Blaheta R, Hasal M, Michalec Z, Takayama Y, Lee Ch, Lee J, Kim GY, Kuo ChW, Kuo WJ, Lin ChYi. DECOVALEX-2019. Task D: INBEB. Final Report. LBNL-2001267. Lawrence National Berkeley Laboratory; 2019.

[3] Gens A, Alcoverro J, Blaheta R, Hasal M, Michalec Z, Takayama Y, Lee Ch, Lee J, Kim GY, Kuo ChW, Kuo WJ, Lin ChYi. HM and THM interactions in bentonite engineered barriers for nuclear waste disposal. Int. J. Rock Mech. & Mining Sci; submitted 2020.

[4] Alonso EE et al. The FEBEX benchmark test: Case definition and comparison of modelling approaches. International Journal of Rock Mechanics and Mining Sciences. 2005; 42: 611-638.

[5] Stephansson O, Tsang CF eds. Coupled Thermo-Hydro-Mechanical-Chemical Processes in Geo-Systems: Fundamentals, Modelling, Experiments and Applications. Elsevier Geo-Engineering Book Series. Volume 2; 2004.

[6] Fuentes-Cantillana JL, García-Siñeriz JL. FEBEX: Full-scale engineered barriers experiment in crytalline host rock: Final design and installation of the 'in situ' test at Grimsel. Publicación technica num. 12/98. ENRESA, Madrid; 1998

[7] Alberdi J, Barcala JM, Campos R, Cuevas AM, Fernandez E. FEBEX project: full-scale engineered barriers experiment for a deep geological repository for high level radioactive waste in crystalline host rock. Final report Publicación Técnica 1/2000. ENRESA, Madrid; 2000.

[8] Bárcena I, Fuentes-Cantillana JL, García-Siñeriz JL. Dismantling of heater No. 1 at the FEBEX in situ test. Description of operations. AITEMIN, Madrid 2003.

[9] Lloret A, E. Romero E, Villar MV. FEBEX II Project Final report on thermo-hydro-mechanical laboratory tests. ENRESA, Madrid; 2004.

[10] Huertas F, Farina P, Farias J, Garcıa-Sineriz JL, Villar MV, Fernandez AM, et al. Full-scale engineered barrier experiment. Updated final report, technical publication 05-0/2006. ENRESA, Madrid; 2006.

[11] García-Siñeriz JL, Abós H, Martínez V, De la Rosa C, Mäder U, and Kober F. FEBEX DP: Dismantling of heater 2 at the FEBEX "in situ" test. Description of operations. NAGRA Arbeitsbericht NAB 16-11; March 2016.

[12] Villar MV, Iglesias RJ, Abós H, Martínez V, de la Rosa C, Manchón MA. FEBEX-DP Post-mortem THM/THG Analysis Report. NAB 16-17; 2017.

[13] Villar MV, Gómez-Espina R. Report on Thermo-Hydro-Mechanical Laboratory Tests Performed by CIEMAT on Febex Bentonite 2004-2008. Informes Técnicos Ciemat 1178; 2009.

[14] Rutquist J, Tsang CF. A Fully Coupled Three-Dimensional THM Analysis of the Febex in Situ Test with the Rocmas Code: Prediction of THM Behavior in a Bentonite Barrier. In: [5]. pp 143-148

[15] Gens A, Sánchez M, Guimarães L, Alonso E, Lloret A, Olivella S, Villar M, Huertas F. A full-scale in situ heating test for high-level nuclear waste disposal: Observations, analysis and interpretation. Géotechnique. 2009, 59: 377-399.

[16] Papafotiou A, Kober CLi & F, Qiao YF, Ferrari A, Laloui L, Sánchez M, Gens A, Åkesson M, Pre-dismantling THM modelling of the FEBEX in situ experiment. NAB 16-22; 2017.

[17] Bear J, Cheng AHD. Modeling Groundwater Flow and Contaminant Transport. Springer, Dordrecht; 2010.

[18] Lewis RW, B. A. Schrefler BA. The Finite Element Method in the Static and Dynamic Deformation and Consolidation of Porous Media. 2nd Edition. Wiley J, Chichester; 1998.

[19] Abed AA, Sołowski WT. A study on how to couple thermo-hydro-mechanical behaviour of unsaturated soils: Physical equations, numerical implementation and examples. Computers and Geotechnics. 2017; 92: 132-155.

[20] De Vries DA. Simultaneous transfer of heat and moisture in porous media. Trans. Amer. Geophys. Union: Volume 39; 1958: 909-916.

[21] Wang W, Rutqvist J, Görke UJ, Birkholzer JT, Kolditz O. Non-isothermal flow in low permeable porous media: a comparison of 'Richards' and two-phase flow approaches. Environ Earth Sci. 2011; 62: 1997-1207.

[22] Philip JR, de Vries DA. Moisture Movement in Porous Materials under Temperature Gradients. Transactions, American Geophysical Union. Vol. 38; 1957. pp. 222-232.

[23] Duncan JM, Poulos HG. Modern techniques for the analysis of engineering problems in soft clay. Chapter 5 in Soft Clay Engineering, E.W. Brand and R.P. Brenner eds., Elsevier; Amsterdam 1981.

[24] Alonso EE, Gens A, Josa AA. A constitutive model for partially saturated soils. Géotechnique. 1990; 40: 405-430.

[25] Gens A, Constitutive laws. In Modern Issues. In: Non-Saturated Soils, Gens A, Jouanna P, Schrefler BA eds. Springer: Vienna; 1995. pp 129-158.

[26] Chijimatsu M, Börgesson L, Fujita T, Hernelind J, Jussila P, Nguyen TS, Rutqvist L, Jing L. Model development and calibration for the coupled thermal, hydraulic and mechanical phenomena of the bentonite. Environmental Geology. 2008; 57: 1255-1261.

[27] Kröhn KP. Modelling the re-saturation of bentonite in final repositories in crystalline rock. GRS Report, GRS-199; 2004.

[28] Kröhn KP. New evidence for the dominance of vapour diffusion during the re-saturation of compacted bentonite. Engineering Geology. 2005; 82: 127-132.

[29] Idiart A, Pekala M. Models for Diffusion in Compacted Bentonite. SKB TR-15-06, SKB Swedish Nuclear Fuel And Waste Management Co, Stockholm; 2016.

[30] Bradbury MH, Baeyens B. Porewater chemistry in compacted re-saturated MX-80 bentonite. Journal of Contaminant Hydrology. 2003; 61: 329-338.

[31] Villar MV, Lloret A. Influence of dry density and water content on the swelling of a compacted bentonite. Applied Clay Science. 2008; 39: 38-49.

[32] Moldrup P, Olesen T, Rolston DE, Yamaguchi T. Modeling diffusion and reaction in soils.7. Predicting gas and ion diffusivity in undisturbed and sieved soils. Soil Sci. 1997; 162: 632-640.

[33] Moldrup P, Olesen T, Gamst J, Schjønning P, Yamaguchi T, Rolston DE. Predicting the Gas Diffusion Coefficient in Repacked Soil: Water-Induced Linear Reduction Model. Soil Science Society of America Journal. 2000; 64: 1588-1594

[34] Rutquist J. SKI/LBNL Modelling of Task A-1 using ROCMAS. In: Influence of near field coupled THM phenomena on the performance of a spent fuel repository, L. Jing and Son Nguyen eds., DECOVALEX-THMC Project. SKI Report; 2007. pp. 61-72.

[35] Man A, Martino JB. Thermal, Hydraulic and Mechanical Properties of Sealing Materials. NWMO TR-2009-20, Atomic Energy of Canada; 2009.

[36] COMSOL Multiphysics® v. 5.3a. www.comsol.com. COMSOL AB, Stockholm, Sweden; 2018.

[37] Martínez V, Abós H, García-Siñeriz JL. FEBEXe: Final Sensor Data Report (FEBEX "in situ" Experiment). AITEMIN, NAGRA technical report Arbeitsbericht NAB 16-19; 2016.

[38] Schneider S, Mallants D, Jacques D. Determining hydraulic properties of concrete and mortar by inverse modelling. Belgian Nuclear Research Centre; 2012.

[39] Gens A. Additional data for FEBEX experiment which were kindly provided on request.